



Climate change over the high-mountain versus plain areas: Effects on the land surface hydrologic budget in the Alpine area and northern Italy

Claudio Cassardo^{1,2,3}, Seon Ki Park^{2,3,4}, Marco Galli^{1,a}, and Sungmin O^{4,b}

¹Department of Physics and NatRisk Center, University of Torino “Alma Universitas Taurinorum”, Torino, Italy

²Department of Climate and Energy Systems Engineering, Ewha Womans University, Seoul, Republic of Korea

³Center for Climate/Environment Change Prediction Research and Severe Storm Research Center, Ewha Womans University, Seoul, Republic of Korea

⁴Department of Environmental Science and Engineering, Ewha Womans University, Seoul, Republic of Korea

^anow at: Air Force Mountain Centre, Sestola, Modena Province, Italy

^bnow at: Institute for Geophysics, Astrophysics, and Meteorology, University of Graz, Austria

Correspondence to: S. K. Park (spark@ewha.ac.kr)

Abstract. Climate change may intensify during the second half of the current century. Changes in temperature and precipitation can exert a significant impact on the regional hydrologic cycle. Because the land surface serves as the hub of interactions among the variables constituting the energy and water cycles, evaluating the land surface processes is essential to detail the future climate. In this study, we employ a trusted Soil-Vegetation-Atmosphere Transfer scheme, called the University of Torino model of land Processes Interaction with Atmosphere (UTOPIA), in offline simulations to quantify the hydrologic components changes in the Alpine area and northern Italy, on the basis of regional future climate (FC) conditions produced by the Regional Climate Model version 3 (RegCM3) via the IPCC A2 and B2 scenarios. In FCs, the evapotranspiration generally increases, especially over the plain areas, and consequently the surface soil moisture decreases during summer, falling below the wilting point threshold for one more month compared to present climate. In the high-mountain areas, due to the earlier snow melting, the land surface becomes snowless for an additional month. The annual mean number of dry (wet) days increase remarkably (slightly) in FCs; thus increasing the risk of severe droughts, and slightly increasing the risk of floods coincidentally. Our results have serious implications on human life, including agricultural production, water sustainability and general infrastructures, and can be used to plan the managements of water resources, floods, irrigation, forestry, hydropower, and many other relevant activities.

1 Introduction

Based on the results from global climate models (GCMs) in the condition of increasing concentration of greenhouse gases (IPCC, 2007, 2013), the climate change over the end of this century (e.g., increase of the mean temperature and change of the precipitation amount) is expected to occur irregularly in space and time but to mostly affect some specific and critical regions



(Beniston, 2006). Since the Intergovernment Panel on Climate Change (IPCC) Fourth Assessment Report (AR4; IPCC, 2007), these results have been generally confirmed (Goodess et al., 2009), especially concerning southern Europe.

In a generic mesoscale basin, such potential changes will influence hydrologic budget; thus, altering the amount of available water and acting as climate feedback. In addition, the temperature and seasonal precipitation pattern changes can affect the permanent or seasonal snowmelt, thus affecting streamflow timings and then again the water availability. Even where the precipitation will increase, the concurrent warming will favor a further increase of evapotranspiration (ET). The decrease of water supplies, conjunctly with the likely increase of the demand, could significantly influence agriculture (the largest consumer of water) and municipal, industrial and other uses (EEA, 2005). Nevertheless, to evaluate locally the net effect of changing climate on water resources, the hydrologic budget must be detailed (Bocchiola et al., 2013).

Annual or seasonal variations of temperature and precipitation also drive changes in runoff and streamflow: for instance, the peak streamflow may occur earlier than now in places where snowpack significantly determines the water availability (IPCC, 2007). Such changes may seriously influence the water and flood management, often with significant economic consequences, though the resulting effects may differ for regions even at similar latitudes, as evidenced by Adam et al. (2009) for the high latitudes of North America and Eurasia.

Global circulation models represent the large-scale atmospheric and oceanic processes. Even if they include sophisticated atmospheric physics and feedbacks with land surface and ocean conditions, they only show conditions averaged over large areas. Hydrologic processes normally operate at quite smaller scales, i.e., meso- and storm scale in meteorology and basin scale in hydrology, and local conditions can be most extreme than those suggested by the areal mean values (see, e.g., the analysis on the groundwater use and recharge in Crosbie et al., 2005). Several recent studies attempted to evaluate the hydrologic effects of climate changes in individual small-scale catchments using a variety of water balance models and climate change scenarios (e.g., Nemec and Schaake, 1982; Gleick, 1986, 1987; Flaschka et al., 1987; Bultot et al., 1988; Lettenmaier and Gan, 1990; Ayers et al., 1990; Klausmeyer, 2005; Buytaert et al., 2009; Berg et al., 2013). Despite of some differences in results, due to the different forcing data or scenarios used (Rind et al., 1992), they have gathered some suitable information at basin or regional scale.

These studies also reveal that the land surface has been recognized as a critical component for the climate. Key points are the partitioning of solar radiation into sensible and latent heat fluxes, and that of precipitation into evaporation, soil storage, groundwater recharge, and runoff. Despite the increased consideration of such processes, the land surface parameters are not systematically measured at neither large scale nor mesoscale, making it hard to perform hydrologic analyses. To overcome such a problem, we have used a methodology called the CLImatology of Parameters at the Surface (CLIPS), proposed by some other studies (e.g., Cassardo et al., 1997, 2009). According to CLIPS, the output of a land surface scheme is used as a surrogate of surface observations, to estimate the surface layer parameters.

Section 2 includes a schematic summary of models and experiment design. Results concerning the hydrologic budget are reported in Section 3, and conclusions are provided in Section 4.



2 Models and experimental setup

In previous studies, the land surface scheme used in CLIPS was always driven by the meteorological observations. As this study aims at evaluating the climate change effects on the hydrologic budget components, the output of a regional climate model has been selected, for the first time, as input data for CLIPS. Currently, horizontal resolutions of some regional climate models (driven by GCM) become higher than 10 km; it is sufficiently high to infer the general characteristics of the energy/water cycles for large and medium scale basins, though still quite coarse for detailing the hydrologic budget components in a small scale basin.

We have considered three 30-year periods: the reference period 1961–1990 (hereafter referenced to as present climate, or PC), and the last thirty years of the 21st century (2071–2100), referred to as future climate (FC) — FC_{A2} and FC_{B2} based on the IPCC A2 and B2 emission scenarios (Nakicenovic and Swart, 2001), respectively.

For the analyses, we use the data obtained from a chain of model simulations. The land surface parameters are calculated through the University of Torino model of land Processes Interaction with Atmosphere (UTOPIA; Cassardo, 2015), which has been widely used for studies of energy/water cycles and atmosphere-land surface interactions under different regional climate conditions (e.g., Loglisci et al., 2001; Cassardo et al., 2006, 2007, 2009; Galli et al., 2010; Zhang et al., 2011; Francone et al., 2012; Park et al., 2017). Meteorological inputs to UTOPIA are provided by outputs, based on the PC and FC scenarios, from the Regional Climate Model version 3 (Elguindi et al., 2007) — one of the models that participated in the European Union project called the Prediction of Regional scenarios and Uncertainties for Defining European Climate change risks and Effects (PRUDENCE; see <http://prudence.dmi.dk/>). Despite the availability of the products for Europe within the World Climate Research Program Coordinated Regional Downscaling Experiment (EURO-CORDEX; Jacob et al., 2014), the RegCM3 output, also used in other studies in Europe (e.g., Giorgi et al., 2004; Gao et al., 2006), has been selected because it is still well known and is one of the existing datasets with the highest resolution currently available (20 km).

The computational domain occupies most of the Alpine region and northern Italy, including the Po River basin, bordered by $5^{\circ}\text{E} - 15^{\circ}\text{E}$ and $43^{\circ}\text{N} - 48^{\circ}\text{N}$ (Figure 1). A total of 720 grid points are defined in the domain, which are categorized into different areas depending on the grid elevation (h) above sea level (a.s.l.): the plain area ($h \leq 500$ m a.s.l.) and the high-mountain area ($h > 2000$ m a.s.l.).

The UTOPIA has been driven over each grid point using the following RegCM3 output: temperature, humidity, pressure and wind at the surface level, precipitation, and short- and long-wave radiation. To ensure the numerical stability of UTOPIA, all 3-hourly RegCM3 outputs (except precipitation) have been interpolated every hour using a cubic spline, whereas precipitation has simply been redistributed assuming a constant rate.

A total of 10 soil layers are set in the UTOPIA simulations, for a total soil depth of about 51 m. Soil thickness starts from the surface layer of 0.05 m, then progressively doubles up to the lowest layer, about 25 m deep, which may be interpreted as a boundary relaxation zone. More specifically, the bottom-level depth of each layer, from layer 1 (top) to layer 10 (bottom), is set to 0.05, 0.15, 0.35, 0.75, 1.55, 3.15, 6.35, 12.75, 25.55, and 51.15 m. Soil characteristics are taken from ECOCLIMAP



(Masson et al., 2003), and initial values of soil moisture and temperature are set following Cassardo (2015). Short grasses are assumed to cover the whole domain.

3 Results

5 The multiple simulations performed for PC and FCs are presented in terms of the temporal and spatial variability by displaying time series (annual cycles) and 2-dimensional maps, respectively, of the mean values of some variables. For time averaging, Xu and Singh (1998) suggested to use monthly mean values for discussing the hydrologic budget variations induced by climate change; however, we preferred a period of 10 days to better quantify time shifts of the physical variables. In this study, the annual cycles are figured via the 10-day averages over the 30-year simulation period, at each elevation-categorized grid-point
10 set. Each month has three 10-day periods: days 1 to 10, 11 to 20, and 21 to the end of the month.

The analyzed variables include precipitation (PR), evapotranspiration (ET), surface runoff (SR), and soil moisture (SM). We noticed that the general trends of annual cycles are similar between PC and FCs. Therefore, in order to accentuate the extent and direction of changes, the future variations of the hydrologic budget components are shown as the differences between FCs and PC; the PR difference (ΔPR) represents PR_{FC} minus PR_{PC} , where FC is either FC_{B2} or FC_{A2} — similarly to ΔET and
15 ΔSR .

In this study, SM is defined as the quantity of water contained in soil that is composed of solid particles, air and water, and is represented as saturation ratio (S):

$$S = \frac{V_w}{V_w + V_a} = \frac{V_w}{V_v}, \quad (1)$$

where V_w , V_a and V_v are the volumes of water, air and voids, respectively, in soil.

20 3.1 Evapotranspiration, Precipitation and Soil Moisture: Temporal Variability

Figure 2 compares the annual cycle of PR, ET and SR in the plain area ($h \leq 500$ m a.s.l.). In the PC summer, ET exceeds PR from the end of June (when ET peaks to about 22 mm) to the end of August (when SM is minimum $\sim 0.52 \text{ m}^3 \text{ m}^{-3}$; see Figure 3). PR shows its minimum between mid-June and August when it is lower than ET. In the PC winter, PR is much higher than ET, and SR exceeds ET from October to March. In the summers of FCs, ET exceeds PR for a longer period (in FC_{A2}), and both
25 scenarios show larger water deficits in July and August, with the PR minimum shifted to August in FC_{A2} . Furthermore, the ET maxima shift towards July/August, in both FC_{A2} and FC_{B2} , and the values increase by as much as 3–5 mm (i.e., ΔET s).

It is conspicuous that the summer PR decreases in future — between the end of May and the beginning of September in FC_{B2} (Figure 2b), and between July and September in FC_{A2} (Figure 2c). On the contrary, PR generally increases in winter, between December and February, in both FCs. In autumn, ΔPR s show large variations in short periods: for instance, in FC_{B2} ,
30 it varies as -6 mm in mid-September, $+10$ mm in late September, -12 mm in late October, $+15$ mm in mid-November, and -7 mm in late November. Regarding ΔET , there are almost no variations in cold months, while there is a small increment (up



to 3 mm) between April and September in FC_{B2} , and a larger increment in the same period in FC_{A2} , with the largest value in August (~ 5 mm).

Figure 3 shows the 10-day mean values of SM for the plain area, expressed as saturation ratio — see Eq. (1). Variations of SM in plains are almost negligible in a colder period (late November – mid-May), but are large during a warmer period (late May – mid-November): the driest points are antedated by ~ 10 days in FCs, still being in August, and their values decrease by $\sim 0.1 \text{ m}^3 \text{ m}^{-3}$. The decrease begins already in spring (from late May) and continues till late October (FC_{B2}) or early November (FC_{A2}), with the largest depletion in early August (FC_{B2}) and in early to mid- August (FC_{A2}). Moreover, the period that future SM values are lower than the lowest SM of PC (i.e., $\sim 0.52 \text{ m}^3 \text{ m}^{-3}$ in mid-August) extends from early July to early September in FC_{B2} and to mid-September in FC_{A2} . In the driest periods of FCs, several grid points in the plains go below their permanent wilting points (PWP), which vary according to soil type, or remain below PWP for an excessive duration by about one month.

Our results regarding the future changes of SM in the warm period — an increase in days of SM lower than the lowest SM of PC, and a surplus of period below PWP — signify that, if the land use of the grid points is pasture, we need appropriate countermeasures to ensure an adequate productivity. During the cold period in plains, SM shows the highest values ($\sim 0.73 \text{ m}^3 \text{ m}^{-3}$) in both PC and FCs; the SM values of FCs slightly exceed those in PC, due to the small increments of PR in this period (see Figures 2b and c).

Figure 4 shows the annual cycle of hydrologic budget components over the high-mountain area ($h > 2000$ m a.s.l.). In both PC and FCs, PR does not exceed ET while the gap between the two variables narrows in the FC summers, due to an increase in ET and a decrease in PR. In PC, ET peaks in mid-July while PR peaks in late June. The peak of SR, between May and June, is out of phase because it is also affected by the concurrent snow melting. It is noteworthy that PRs in summer and fall generally decrease in FCs (i.e., $\Delta PR < 0$) from mid-June to mid-November: except for short terms in early July, from mid- to late August and from late September to late October in FC_{B2} , and except only from early October to early November in FC_{A2} . On the contrary, in winter and spring, PRs generally increase in FCs from mid-January to early June except for short-term decreases in mid-April and mid-May. Regarding ΔET , there are almost no variations in cold months, whereas there is a large increment (~ 10 mm) between May and June, and a low-to-moderate increment (~ 2 – 6 mm) between July and October in FCs.

Finally, for ΔSR at high mountains, there is a weak increase (< 5 mm) between late November and late March, a stronger increment (~ 10 mm) in April, especially in FC_{B2} , a strong decrease (up to -25 to -31 mm) between May and June, and a general weak decrease in summer between July and September (see Figures 4b and c). As a result, the maxima of SR in FCs significantly decrease and their occurrence dates shift ahead to May for FC_{B2} and between April and May for FC_{A2} because snow melting occurs nearly 30–40 days earlier — see also the analysis on frost frequency in Galli et al. (2010). These variations are in line with the changes of snowpack, which starts to melt earlier, between late April and early May, in FCs. Such results also agree with other studies, carried out using regional climate models on the Alpine areas: for example, Lautenschlager et al. (2008), for PR and ET, and Jacob et al. (2007), for snow. Note that SR in PC is almost null between mid-December to March while ΔSR s in FCs in the same period are positive: this indicates the presence of rainfalls and/or snow melting over at least some parts of the high-mountain grid points, even in the coldest periods.



Figure 5 shows SM at the high-mountain grid points and demonstrates the effects of hydrologic budget components on surface SM. We note that the behaviors of SM at high mountains are substantially different from those at plains (cf. Fig. 3). In PC, the highest SM ($\sim 0.65 \text{ m}^3 \text{ m}^{-3}$) occurs at early June while the lowest SM ($\sim 0.51 \text{ m}^3 \text{ m}^{-3}$) arises at early to mid-March. The increase in SM from late March to early June is related to snow melting due to increase in net radiation. Surface SM in PC starts to decrease as the cold season starts in early November, reaching the minimum in mid-March. Note that SMs during the same cold period in FCs are larger than SM in PC, evidencing a larger amount of liquid precipitation in FCs: in other words, winter rainfalls will be more frequent in the future. The peak of SM in spring is advanced by 10–20 days in FC, occurring in early May. The magnitude of maximum SM in FC is a bit lower than that in PC but the spread is larger, implying that snow ablation starts much earlier and lasts longer. In addition, the occurrence of the minimum SR shifts from mid-March in PC to summer in FC: in both February and early August (i.e., two minima) in FC_{B2} , and late August in FC_{A2} . This shifting is mainly caused by the enhancement of ET.

3.2 Evapotranspiration, Precipitation and Soil Moisture: Spatial Distribution

Our analyses illustrates that the differences in the SM behaviors between PC and FC, at both plains (Figure 3) and high mountains (Figure 5), are strongly linked to the variations of the hydrologic budget components. In this section, to understand such linkage more clearly, we perform analyses on the spatial distribution of hydrologic variables (i.e., PR, ET, SR and surface SM) along with discussions on the associated energy variables (i.e., net radiation (NR) and surface soil temperature (ST)), during summer when such variables generally show their largest values.

Figure 6 shows the variables averaged in the month of July, in which PR and surface SM are close to their annual minima while ET is close to its annual maximum. Here, we discuss the variables in terms of anomalies of FC_{A2} only because of similar patterns to but larger variations than those of FC_{B2} . Variables in Figure 6 are anomalies of hydrologic budget components: ΔET , ΔPR , ΔSR and ΔSM where, e.g., ΔET represents $\text{ET}_{\text{FC}_{A2}} - \text{ET}_{\text{PC}}$.

Compared to PC, we notice a large increment of NR everywhere in FC_{A2} (not shown), with the exception of few grid points located in the central and western Alps. Regarding ΔET (Figure 6a), plains along the Po River and the northern off-alpine regions (i.e., middle-slope and/or foot) show the largest increments, well correlated to ΔNR , implying that most of the available energy excess is used for evaporative processes. In contrast, on the Apennines and central Alps, ΔETs are almost null or slightly negative while ΔNRs are insignificantly positive. ΔPR (Figure 6b) and ΔSR (Figure 6c) show similar signals, with a general deficit, especially on the eastern and western Alpine areas. Surface ΔSM (Figure 6d) shows a general reduction, larger in the zones at latitudes lower than 45°N , whereas surface ΔST (not shown) is almost uniformly larger in the considered domain. As ETs increase (i.e., $\Delta\text{ET} > 0$), SMs generally decrease; however, both decrease over some regions where ΔSMs are strongly negative — on the western mountainous Emilia Romagna region and Tuscany, and along the Po River and in central and southern Piemonte as well (cf. Figures 6a and 6d). When SM decreases below the wilting point, evaporation generally ceases because there is no available water for further ET, and the ET anomaly (i.e., ΔET) can be negative. Considering that most of those areas are important for agricultural production (see, e.g., Prino et al., 2009, a study on grapevine in Piemonte region), our results constitute a threatening challenge for future agricultural productivity.



It is evident that ΔET and ΔPR do not show a linear correlation (cf. Figures 6a and 6b). ΔET s are generally positive, whereas ΔPR s are distributed around null with some positive peaks on the Apennines and northwestern Italy and large negative peaks on some Alpine locations. This disparity brings about and/or enhances the nonlinear interactions among temperature, evaporation, soil moisture, etc. Noting that nonlinearity can develop even with small perturbations (e.g., Park, 1999), our results elucidate that similar investigations can only be conducted using models that are able to give a correct estimation of energy and hydrologic processes.

5 3.3 Number of Wet and Dry Days in the Future Climate

The availability of the SM estimations enables us to evaluate the occurrence of dry and wet days, instead of using relative humidity as usual, in a similar way to figure the warm and cold days via the ST estimations. We employ SM to assess the dry and wet days in FCs because it is a more valuable indicator of the soil hydrologic conditions and directly reflects the hydrologic status of the soil water, e.g., used by plants. Here, we limit the analysis to the surface SM (i.e., in the top soil layer with a depth of 5 cm), due to its significant impact on several agricultural productions.

In order to find the absolute thresholds for SM, we have selected two parameters: PWP and the field capacity. PWP is the SM level below which the osmotic pressure of the plant roots is insufficient to extract water from the soil, and is usually considered as an indicator of a serious water deficit for agricultural practices. The field capacity represents the SM level above which the gravitational drainage, due to soil hydraulic conductivity, causes a rapid removal of the excessive water through percolation into deeper layers; thus it is considered as a threshold above which soil is very wet, as in the cases of very intense precipitations, sometimes causing floods. Since these two values change according to the soil type and texture, we define a non-dimensional index, Q_I , which is independent from soil type, as:

$$Q_I = \frac{q_1 - q_{wi}}{q_{fc} - q_{wi}} \quad (2)$$

where q_1 is the moisture of the top soil layer, q_{wi} is PWP and q_{fc} is the field capacity. All the values are expressed in the unit of soil saturation ratio. In this way, the soil wetness is categorized in terms of Q_I as: extremely dry soil for $Q_I \leq 0$, and extremely wet soil for $Q_I \geq 1$. In this study, we define the thresholds for dry soil and wet soil as $Q_I = 0$ and $Q_I = 0.8$, respectively. Note that it is quite rare to see the cases with $Q_I = 1$ because the 3-hourly precipitation data from RegCM3 are interpolated to hourly data by keeping the constant rain rate, to be used as input for UTOPIA. Therefore, we have arbitrarily defined the threshold for wet soil as $Q_I = 0.8$.

Figure 7 shows the anomalies of dry and wet days in FC_{A2}. The number of dry days generally increase in most of the domain except the Alpine high-mountain areas (Figure 7a). Higher number of dry days (e.g., 30–50 days) occur over the regions of extreme soil dryness — the coastal areas as well as the off-alpine regions of the Alps and the Apennines (cf. Figure 6d). The interannual variability of the dry-day occurrence also decreases (not shown), implying that our results are relatively robust and that we may experience drought over the non-high-mountain areas in almost every year.

The number of wet days, on the other hand, is almost stationary over plains but increases by 10–15 days in some localized regions close to the Alps in the Italian side (especially in the Lombardy region), and by even more than 20 days at the feet



of the Alps in Switzerland, France and Austria (Figure 7b). The interannual variability is generally stationary, but increases in the areas with the largest numbers of wet days (not shown). Therefore, in FC_{A2} , we can have more occasions of reaching high values of surface SM, hence potentially higher risk of floods. This also implicates corresponding higher possibility of hydrogeological instability over the same areas of higher flood risk.

5 4 Conclusions

In this study, we investigated the characteristic changes of hydrologic budget components and soil moisture, over the Alpine areas and northern Italy under future climate (FC) conditions, by employing the University of TORino model of land Processes Interaction with Atmosphere (UTOPIA) in offline simulations. The meteorological input data in FCs are provided by the Regional Climate Model version 3 (RegCM3), based on the IPCC A2 and B2 scenarios.

10 In FCs based on the A2 and B2 scenarios (FC_{A2} and FC_{B2} , respectively), the most significant changes are the increment of evapotranspiration (ET) and the subsequent depletion of soil moisture (SM), more remarkably in FC_{A2} . Precipitation (PR) shows the lowest values while ET depicts the highest values in the future summer (in particular, July), when SMs are the lowest in many grid points. In the plain area, the minimum SM in FC occurs about 20–30 days earlier than in the present climate (PC), and remains low for the successive months up to November. In the high-mountain area, the surface runoff (SR) coming from
 15 the snow melting keeps the soil water amount sufficiently high to maintain the ET levels high from May to October, especially in FC_{A2} ; thus, ET (or latent heat flux) always exceeding sensible heat flux (SHF). In plains, the period in which ET exceeds PR elongates by about one month, mainly in spring. Moreover, SM decreases also for one more month in summer, falling below the wilting point threshold in the surface soil layer. In high mountains, due to the earlier occurrence of snow melting, the land surface becomes snowless for an additional month.

20 We found that these changes in the hydrologic budget components are strongly related to the variations of net radiation (NR), which generally increase in the Alpine area, causing the warming of both the top soil layer and the soil surface — the former through an enhanced SHF, and the latter due to the highest soil heat flux. Under the future conditions of increasing NR and soil temperature along with decreasing SM, we expect two climatic feedbacks to take place: 1) a drier soil brings about higher albedo, and 2) a warmer soil emits more long-wave radiations. Both feedbacks act to decrease NR eventually — i.e., negative
 25 feedbacks. However, there are coincident increments of SHF to the atmosphere as well as longwave radiation emitted by the warmer atmosphere. The overall outcome cannot be generalized because it depends on the intensity of individual component of the energy and hydrologic budgets. This confirms that the climate system is quite complex and that, to evaluate well the surface conditions, it is essential to calculate the energy and hydrologic budget components in detail.

The values presented in this study refer only to the average conditions; however, considering the large interannual variability
 30 of hydrologic variables registered over those areas in PC, we expect to have more frequent and intenser occurrences of longer dry spells (hence severe droughts) and heat waves in FCs, especially in middle summers. As most agricultural products intensively grow in summer (e.g., wheat, rice, maize and grapevine, and other typical products in the Po valley), the potential conditions of elongated drought will exert significantly unfavorable impacts on agricultural production (Bocchiola et al., 2013).



Other activities related to water supply (e.g., industry, hydroelectric power production, etc.) can also suffer serious problems, consequently exerting harmful impacts on economy and human health in local regions.

On the contrary, during winter, PRs generally increase in FCs, with a larger number of the liquid precipitation events at high elevations. Furthermore, in spring, snow melting occurs earlier by about one month, thus resulting in precedence of the SR peak by about 20–30 days. In winter, the SR amount generally increases. By taking into account the large interannual variability of PR, this runoff increases the occurrence and/or duration of wet periods (e.g., heavy rainfalls and floods) during winter and spring in FCs.

We also examined potential changes in dry and wet days in FC_{A2} by analyzing surface SMs. Our results report a higher possibility of having SMs below the wilting point in the plain and coastal areas, and a probability of slightly increasing wet days, particularly in the off-alpine areas.

We note that the numerical values of all variables are dependent on the performance of employed model. Recent studies demonstrate that the land surface processes diagnosed by land surface models are sensitive to vegetation dynamics and variations, and that their accuracy can be further improved by considering various aspects of vegetation effects in the subgrid-scale parameterizations (e.g., Park and Park, 2016; Gim et al., 2017). Moreover, the model uncertainties can be significantly reduced by optimal estimation of the parameter values in the schemes (e.g., Lee et al., 2006; Yu et al., 2013) and/or seeking for an optimized set among multiple-physics optional schemes (e.g., Hong et al., 2014, 2015). By applying these methods, the details of model-generated spatial/temporal changes in the future energy and hydrologic budgets can be different from the current results; however, we believe that the general trends are not significantly disparate. Overall, our findings can provide a useful guideline to plan the managements of water resources, floods, irrigation, forestry, hydropower, and many other activities relevant for human life.

Data availability. The ECOCLIMAP data is available online from <https://opensource.umr-cnrm.fr/projects/ecoclimap>.

Competing interests. The authors declare that they have no conflict of interest.

Acknowledgements. The authors acknowledge the Earth System Physics Section of the ICTP, Italy, for providing the RegCM3 dataset. S. O was partly supported by the University of Torino (UT) for visiting its Department of Physics under the World Wide Style grant. C. Cassardo and S. K. Park are supported by the governments of Italy and Korea, respectively, for visiting each institution for collaborative research via the bilateral scientific agreements. This work is partly supported by the National Research Foundation grant (No. 2009-0083527) funded by the Korean government (MSIP). It was also partly supported by the Ewha Womans University Research Grant of 2016.



References

- Adam, J. C., Hamlet, A. F., and Lettenmaier, D. P.: Implications of global climate change for snowmelt hydrology in the twenty-first century, *Hydrol. Proc.*, 23, 962–972, 2009.
- Ayers, M.A., Wolock, D.M., McCabe, G.J., and Hay, L.E.: Hydrologic effects of climatic change in the Delaware River basin, in: U.S. Geological Survey Yearbook, Fiscal Year 1989, U.S. Government Printing Office, Washington, DC, USA, 31–33, 1990.
- Beniston, M.: Mountain weather and climate: A general overview and a focus on climatic change in the Alps, *Hydrobiol.*, 562, 3–16, 2006.
- Berg, P., Moseley, C., and Haerter, J.O.: Strong increase in convective precipitation in response to higher temperatures, *Nature Geosci.*, 6, 181–185, doi:10.1038/ngeo1731, 2013.
- Bocchiola, D., Nana, E., and Soncini, A.: Impact of climate change scenarios on crop yield and water footprint of maize in the Po valley of Italy, *Agricul. Water Manag.*, 116, 50–61, 2013.
- Bultot, F., Coppens, A., Dupriez, G.L., Gellens, D., and Meulenberghs, F.: Repercussions of a CO₂ doubling on the water cycle and on the water balance – a case study for Belgium, *J. Hydrol.*, 99, 319–347, 1988.
- Burden, R.L. and Faires, J.D.: Numerical Analysis, Brooks/Cole, Boston, MA, USA, 2004.
- Buytaert, W., Celleri, R., and Timbe, L.: Predicting climate change impacts on water resources in the tropical Andes: Effects of GCM uncertainty, *Geophys. Res. Lett.*, 36, L07406, doi:10.1029/2008GL037048, 2009.
- Cassardo, C.: The University of Torino model of land Process Interaction with Atmosphere (UTOPIA) version 2015, Tech. Rep., CCCPR/SSRC-TR-2015-1, CCCPR/SSRC, Ewha Womans University, Seoul, Republic of Korea, 2015.
- Cassardo, C., Ruti, P.M., Cacciamani, C., Longhetto, A., Paccagnella, T., and Bargagli, A.: CLIPS experiment. First step: model intercomparison and validation against experimental data, *MAP Newsletters*, 7, 74–75, 1997.
- Cassardo, C., Loggisci, N., Paesano, G., Rabuffetti, D., and Qian, M. W.: The hydrological balance of the October 2000 flood in Piedmont, Italy: Quantitative analysis and simulation, *Phys. Geogr.*, 27, 411–434, 2006.
- Cassardo, C., Mercalli, L., and Cat Berro, D.: Characteristics of the summer 2003 heat wave in Piedmont, Italy, and its effects on water resources, *J. Korean Meteor. Soc.*, 43, 195–221, 2007.
- Cassardo, C., Park, S.K., Thakuri, B.M., Priolo, D., and Zhang, Y.: Soil surface energy and water budgets during a monsoon season in Korea, *J. Hydrometeor.*, 10, 1379–1396, 2009.
- Crosbie, R.S., Binning, P., and Kalma, J.D.: A time series approach to inferring groundwater recharge using the water table fluctuation method, *Water Resour. Res.*, 41, W01008, doi:10.1029/2004WR003077, 2005.
- EEA: Regional Climate Change and Adaptation. The Alps Facing the Challenge of Changing Water Resources, European Environment Agency, Copenhagen, Denmark, 2009.
- Elguindi, N., Bi, X., Giorgi, F., Nagarajan, B., Pal, J., Solmon, F., Rauscher, S., and Zaakey, A.: RegCM version 3.1 user's guide, Tech. Rep., ICTP, Trieste, Italy, 2007.
- Flaschka, I.M., Stockton, C.W., and Boggett, W.R.: Climatic variation and surface water resources in the Great Basin region, *Water Resour. Bull.*, 23, 47–57, 1987.
- Francone, C., Cassardo, C., Richiandone, R., and Confalonieri, R.: Sensitivity analysis and investigation of the behaviour of the UTOPIA land-surface process model: A case study for vineyards in northern Italy, *Bound.-Layer Meteorol.*, 144, 419–430, 2012.
- Galli, M., Oh, S., Cassardo, C., and Park, S.K.: The occurrence of cold spells in the Alps related to climate change, *Water*, 2, 363–380, 2010.



- Gao, X.J., Pal, J.S., and Giorgi, F.: Projected changes in mean and extreme precipitation over the Mediterranean region from a high resolution double nested RCM simulation, *Geophys. Res. Lett.*, 33, 1–4, 2006.
- Gim, H.-J., Park, S.K., Kang, M., Thakuri, B.M., Kim, J., and Ho, C.-H.: An improved parameterization of the allocation of assimilated carbon to plant parts in vegetation dynamics for Noah-MP, *J. Adv. Model. Earth Syst.*, doi:10.1002/2016MS000890, 2017.
- 10 Giorgi, F., Bi, X., and Pal, J.S.: Mean interannual variability and trends in a regional climate change experiment over Europe. II: climate change scenarios (2071–2100), *Clim. Dyn.*, 23, 839–858, 2004.
- Gleick, P.H.: Methods for evaluating the regional hydrologic impacts of global climatic changes, *J. Hydrol.*, 88, 97–116, 1986.
- Gleick, P.H.: The development and testing of a water balance model for climate impact assessment: modelling the Sacramento basin, *Water Resour. Res.*, 23, 1049–1061, 1987.
- 15 Goodess, C.M., Jacob, D., Déqué, M., Guttierrez, J. M., Huth, R., Kendon, E., Leckebusch, G.C., Lorenz, P., and Pavan, V.: Downscaling methods, data and tools for input to impacts assessments, in: *ENSEMBLES: Climate Change and its Impacts: Summary of research and results from the ENSEMBLES project*, edited by: van der Linden, P. and Mitchell, J. F. B., Met Office Hadley Centre, UK, 59–78, 2009.
- Hong, S., Yu, X., Park, S.K., Choi, Y.-S., and Myoung, B.: Assessing optimal set of implemented physical parameterization schemes in a multi-physics land surface model using genetic algorithm, *Geosci. Model Dev.*, 7, 2517–2529, 2014.
- 20 Hong, S., Park, S.K., and Yu, X.: Scheme-based optimization of land surface model using a micro-genetic algorithm: Assessment of its performance and usability for regional applications, *Sci. Online Lett. Atmos.*, 11, 129–133, 2015.
- IPCC: *Climate Change 2007: The Physical Science Basis. Contribution of Working Group I to the Fourth Assessment Report of the Intergovernmental Panel on Climate Change*, edited by: Solomon, S., Qin, D., Manning, M., Chen, Z., Marquis, M., Averyt, K.B., Tignor, M., and Miller, H.L., Cambridge University Press, Cambridge, UK, 2007.
- 25 IPCC: *Climate Change 2013: The Physical Science Basis. Contribution of Working Group I to the Fifth Assessment Report of the Intergovernmental Panel on Climate Change*, edited by: Stocker, T.F., Qin, D., Plattner, G.-K., Tignor, M., Allen, S.K., Boschung, J., Nauels, A., Xia, Y., Bex, V., and Midgley, P.M., Cambridge University Press, Cambridge, UK, 2013.
- Jacob, D., Göttel, H., Kotlarski, S., and Lorenz, P.: Mögliche Klimaänderungen im Alpenraum, in: *Klimawandel in den Alpen: Fakten – Folgen – Anpassung*, Bundesministerium für Umwelt, Naturschutz und Reaktorsicherheit, Berlin, Germany, 22–27, 2007.
- 30 Jacob, D., Petersen, J., Eggert, B., Alias, A., Christensen, O.B., Bouwer, L.M., Braun, A., Colette, A., Déqué, M., Georgievski, G., Georgopoulou, E., Gobiet, A., Menut, L., Nikulin, G., Haensler, A., Hempelmann, N., Jones, C., Keuler, K., Kovats, S., Kröner, N., Kotlarski, S., Kriegsmann, A., Martin, E., van Meijgaard, E., Moseley, C., Pfeifer, S., Preuschmann, S., Radermacher, C., Radtke, K., Rechid, D., Rounsevell, M., Samuelsson, P., Somot, S., Soussana, J.-F., Teichmann, C., Valentini, R., Vautard, R., Weber, B., and Yiou, P.: EURO-CORDEX: new high-resolution climate change projections for European impact research, *Reg. Environ. Change*, 14, 563–578, 2014.
- 35 Klausmeyer, K.: Effects of climate change on the hydrology of upper Alameda Creek, UC Berkeley: Water Resources Center Archives, Retrieved from: <http://escholarship.org/uc/item/3tz1153d>, 2005.
- Lautenschlager, M., Keuler, K., Wunram, C., Keup-Thiel, E., Schubert, M., Will, A., Rockel, B., and Boehm, U.: Climate simulation with CLM, climate of the 20th century, data stream 3: European region MPI-M/MaD, World Data Center for Climate, 2008.
- Lee, Y.H., Park, S.K., and Chang, D.-E.: Parameter estimation using the genetic algorithm and its impact on quantitative precipitation forecast, *Annal. Geophys.*, 24, 3185–3189, 2006.
- Loglisci, N., Qian, M. W., Cassardo, C., Longhetto, A., and Giraud, C.: Energy and water balance at soil-air interface in a Sahelian region, *Adv. Atmos. Sci.*, 18, 897–909, 2001.



- Lettenmaier, D.P. and Gan, T.Y.: Hydrologic sensitivities of the Sacramento-San Joaquin River Basin, California, to global warming, *Water Resour. Res.*, 26, 69–86, 1990.
- Masson, V., Champeaux, J.L., Chauvin, F., Meriguet, C., and Lacaze, R.: A global database of land surface parameters at 1 km resolution in meteorological and climate models, *J. Clim.*, 16, 1261–1282, 2003.
- 10 Nakicenovic, N. and Swart, R.: *Special Report on Emissions Scenarios: A Special Report of Working Group III of the Intergovernmental Panel on Climate Change*, Cambridge University Press, Cambridge, England, 2001.
- Nemec, J., Schaake, J.: Sensitivity of water resources to climate variations, *J. Hydrol. Sci.*, 27, 327–343, 1982.
- Park, S.K.: Nonlinearity and predictability of convective rainfall associated with water vapor perturbations in a numerically-simulated storm, *J. Geophys. Res.*, 104, 31575–31588, 1999.
- 15 Park, S. and Park, S.K.: Parameterization of the snow-covered surface albedo in the Noah-MP Version 1.0 by implementing vegetation effects, *Geosci. Model Dev.*, 9, 1073–1085, 2016.
- Park, S. K., O, S., and Cassardo, C.: Soil temperature response in Korea to a changing climate using a land surface model, *Asia-Pac. J. Atmos. Sci.*, 53, doi:10.1007/s13143-017-0048-x, 2017.
- Prino, S., Spanna, F., and Cassardo, C.: Verification of the stomatal conductance of Nebbiolo grapevine, *J. Chongqing Univ.*, 8, 17–24, 2009.
- 20 Rind, D., Rosenzweig, C., and Goldberg, R.: Modelling the hydrological cycle in assessments of climate change, *Nature*, 358, 119–123, 1992.
- Xu, C.-Y. and Singh, V.P.: A review on monthly water balance models for water resources investigation and climatic impact assessment, *Water Resour. Manag.*, 12, 31–50, 1998.
- Yu, X., Park, S.K., Lee, Y.H., and Choi, Y.-S.: Quantitative precipitation forecast of a tropical cyclone through optimal parameter estimation in a convective parameterization, *Sci. Online Lett. Atmos.*, 9, 36–39, 2013.
- Zhang, Y., Cassardo, C., Ye, C., Galli, M., and Vela, N.: The role of the land surface processes in the rainfall generated by a landfall typhoon: A simulation of the Typhoon Sepat (2007), *Asia-Pac. J. Atmos. Sci.* 47, 63–77, 2011.
- 370

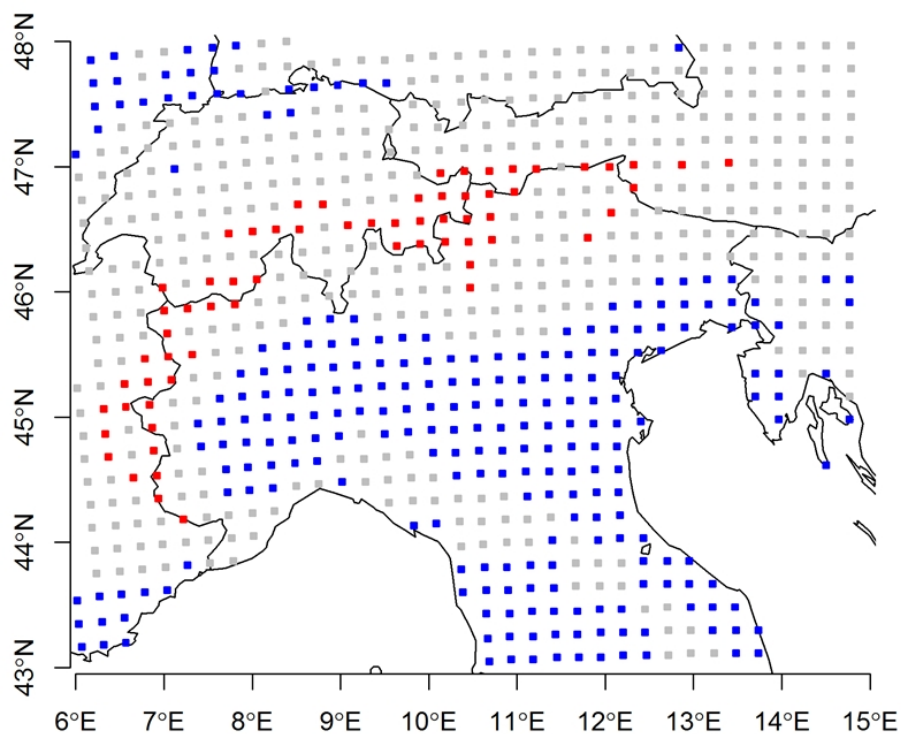


Figure 1. Grid points over the computational domain representing, in terms of the grid elevation (h), the plain area ($h \leq 500$ m a.s.l.; blue), the normal mountains ($500 < h \leq 2000$ m a.s.l.; grey), and the high-mountain area ($h > 2000$ m a.s.l.; red).

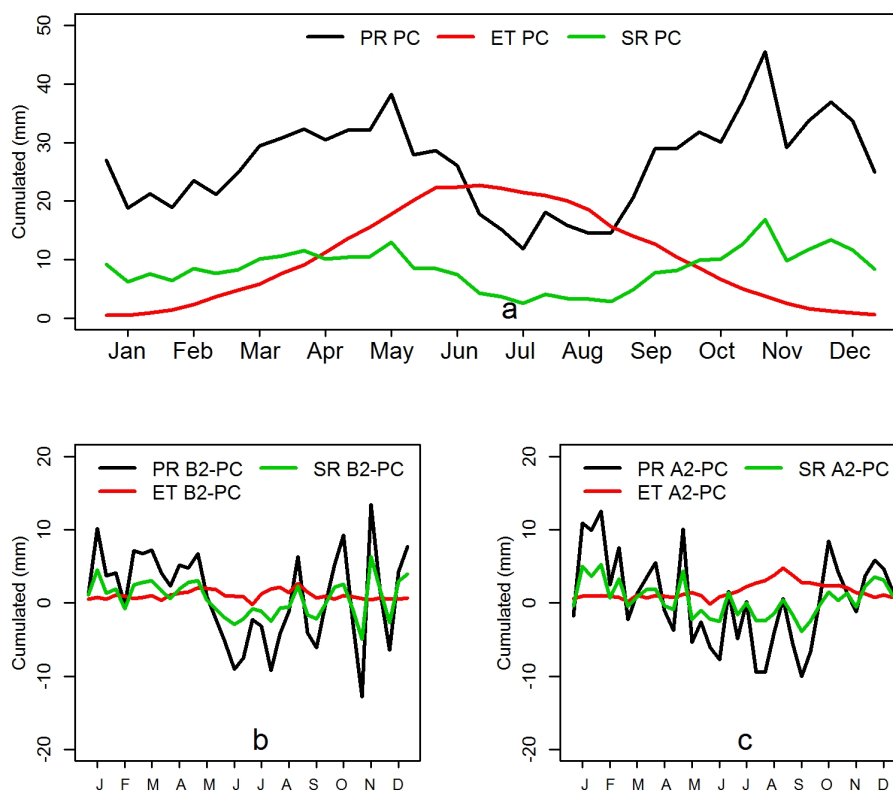


Figure 2. Annual cycles of the 10-day average values of the surface hydrologic budget components for the plain area for a) PC, b) $FC_{B2} - PC$, and c) $FC_{A2} - PC$. Here, PR is precipitation, ET evapotranspiration, and SR surface runoff. Units are mm.

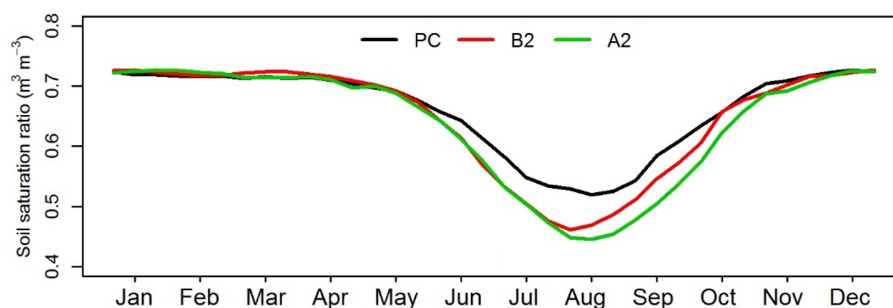


Figure 3. Annual cycles of the 10-day average values of SM, expressed as saturation ratio (in $m^3 m^{-3}$), at the soil surface layer (a depth of 0.05 m) in PC, FC_{B2} , and FC_{A2} for the plain area.

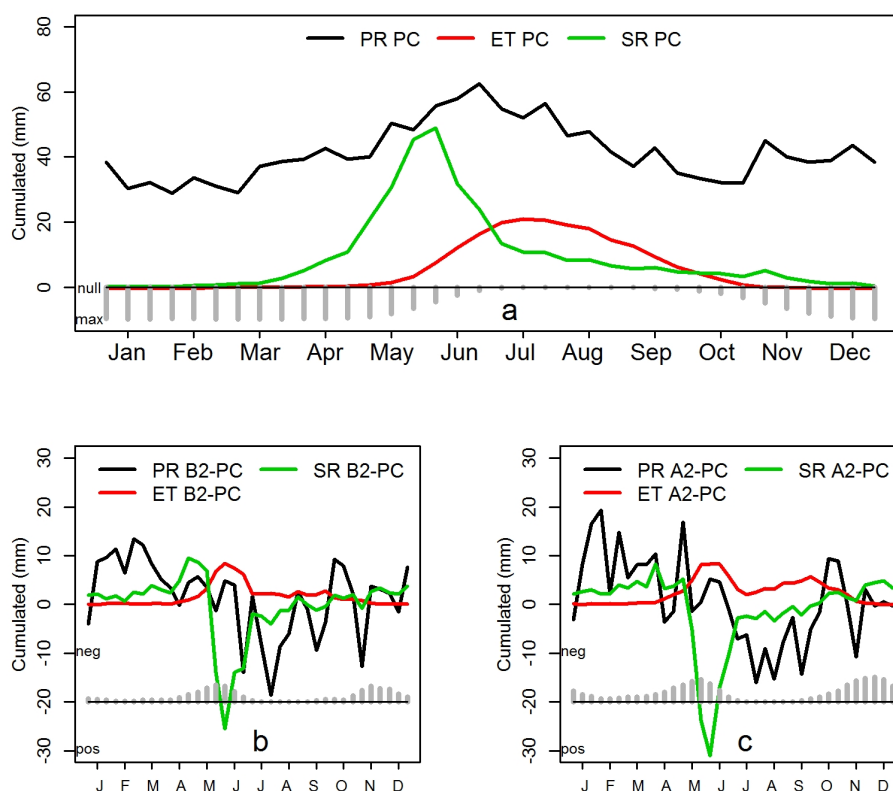


Figure 4. Same as in Figure 2 but for the high-mountain area. Grey bars at the lower portion in a) represent the snow cover (in m) in PC varying from 0 m (null) to 1 m (max); in b) and c) the snow cover difference (in m) between the corresponding FC and PC varying from -1 m (neg) to 1 m (pos). The periods of snow ablation (late spring) and accumulation (mid or late autumn) are well identified.

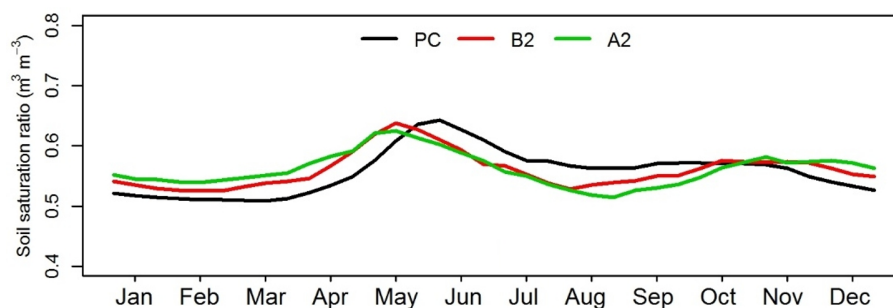


Figure 5. Same as in Figure 3 but for the high-mountain area.

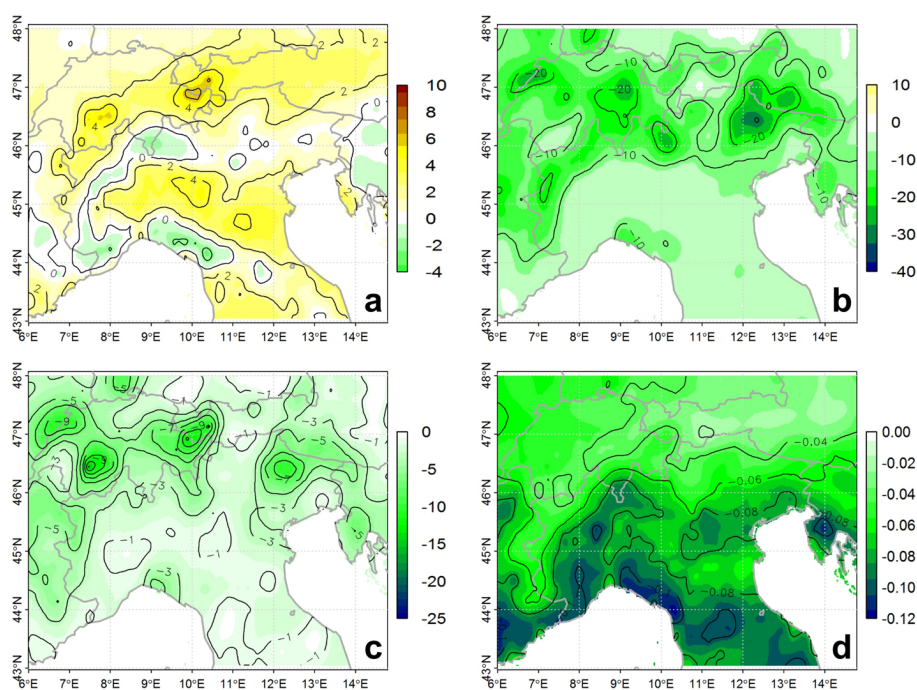


Figure 6. Hydrologic budget components: differences between FC_{A2} and PC (i.e., $FC_{A2} - PC$) of the mean values of a) ET (in mm), b) PR (in mm), c) SR (in mm) and d) surface SM (in $m^3 m^{-3}$). The mean is calculated over the month of July.

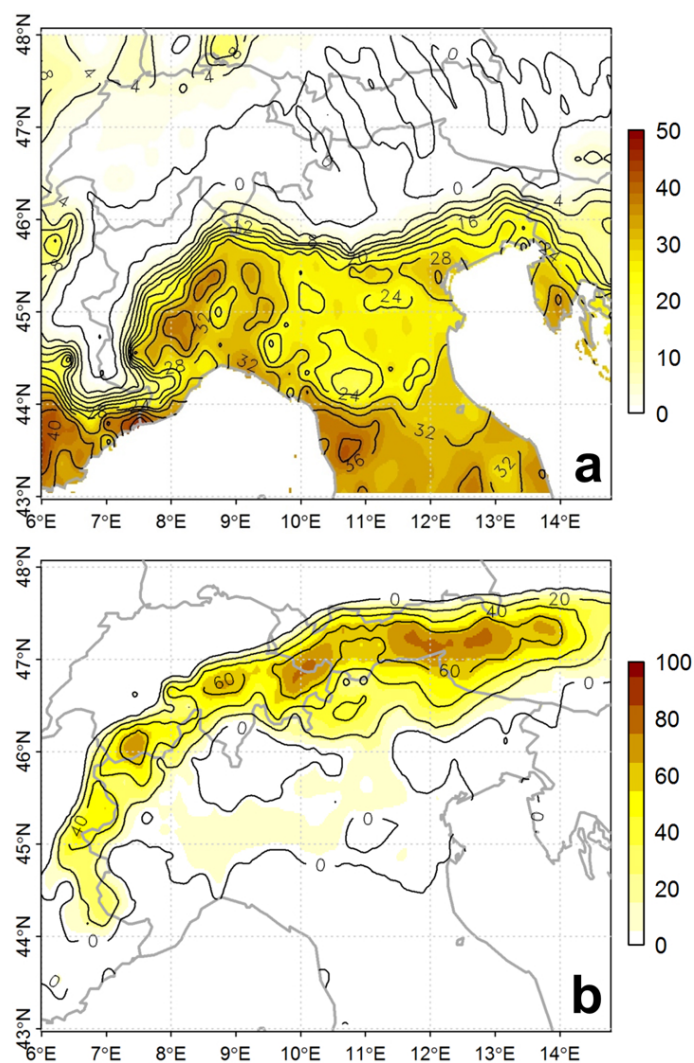


Figure 7. The anomalies of a) dry days and b) wet days in FC_{A2} .